Electronic Supplementary Material (ESI) for ChemComm.

Supplementary information

Multi-cycle reversible control of gas permeability of thin film composite membranes via efficient UV-induced reactions

Abdalrahman U. Alrayyes,[a] Ze-Xian Low,[b] Huanting Wang,*[b] Kei Saito*[a,c]

a. *School of Chemistry, Monash University, Clayton, VIC 3800, Australia Address here.*

b. *Department of Chemical Engineering, Monash University, Clayton, VIC 3800, Australia*

c. *Graduate School of Advanced Integrated Studies in Human Survivability, Kyoto University, Higashi-Ichijo-Kan, Yoshida-nakaadachicho 1, Sakyo-ku, Kyoto, 606-8306, Japan*

Experimental Section/Methods

Penta-erythritol, 11-bromoundecanoic acid, 7-hydroxycoumarin, Karstedt's catalyst, allyl bromide and anhydrous potassium carbonate were all supplied by Sigma Aldrich (Sydney, Australia). p-Toluenesulfonic acid was supplied by Ajax Chemicals (Sydney, Australia). Tetrakis(trimethylsilyloxy)silane was purchased from Gelest, Inc. (PA, USA). Sylgard 184, used for making PDMS, was supplied as a set of curing agent and base agent by Sigma Aldrich (Sydney, Australia). Said chemicals were used without further purification. Low density Polyethylene sheets of 0.03 mm thickness were supplied by Goodfellow (USA).

Synthesis of 7-(allyloxy)coumarin

This material was synthesized following a method previously reported.[1]

*Synthesis of tetrakis(dimethyl(3-((2-oxo-2H-chromen-7-yl)oxy)propyl)silyl) silicate (**4ASil**):*

7-(allyloxy)coumarin (1.15 g, 5.76 mmol) and Tetrakis(dimethylsiloxy)silane (0.187 g, 0.576 mmol) were dissolved in toluene (10ml) by stirring for 1 hour. Karstedt's catalyst (70 µl) was then added and the mixture was stirred at 70 ^{o}C for 3.5 hours. Once the reaction was complete, the solvent was evaporated, and the product was purified by column chromatography (70:30 hexane:ethyl acetate). The reaction scheme is presented in Fig. S2. Reaction yield: 99%, total hydrosilylation products yield: 42%. HRMS (ESI): *m/z* $[M + H]^+$ calcd for $C_{56}H_{68}O_{16}Si_5$, 1137.3426; found, 1137.3432. ^{1}H-NMR δH (600 MHz; CD_2Cl_2): 0.02-0.2 (24H, m, -Si(**CH$_3$**)$_2$), 0.68 (8H, m, -Si(CH$_3$)$_2$**CH$_2$**CH$_2$CH$_2$O-), 1.83 (8H, m, -Si(CH$_3$)$_2$CH$_2$**CH$_2$**CH$_2$O-), 3.97 (8H, t, -Si(CH$_3$)$_2$CH$_2$CH$_2$**CH$_2$**O-), 6.16 (4H, d, ArH), 6.81 (8H, , ArH), 7.34 (4H, d, ArH), 7.62 (4H, d, ArH). IR (cm^{-1}): 2952 (CH), 1703 (C=O), 1610 (C=C), 1565 (C=C), 1123 (SiO), 886 (SiOCH$_3$), 833 (SiOCH$_3$).

Preparation of porous low density polyethylene (LDPE)

Porous LDPE was prepared using a modified thermally induced phase separation (TIPS) method. A 5 ml casting solution was prepared by mixing p-xylene and cyclohexanone in a 95:5 ratio at 130 ^{o}C. 0.5 g of LDPE was then added to the mixture and kept under stirring for 1 hour. The solution was then dropped onto a petri dish, and placed in an ice bath for 5 minutes. The dish was then placed in a vacuum oven at 25 ^{o}C overnight, and finally at 80 ^{o}C for 3 hours to ensure complete solvent evaporation, as well as to reduce pore size.

Fabrication of the polydimethylsiloxane (PDMS) gutter layer

Porous LDPE was cut into small pieces of 1x1 cm, washed with DI water, and dried. The PDMS solution was prepared by mixing the base and curing agent (Sylgard 184) using a 10:1 base:curing agent ratio in hexane (5 wt.%) for 15 minutes, followed by degassing and sonicating for 15 minutes. The solution was then spin coated onto porous LDPE at 3000 rpm for 40 seconds using the static dispense method, and cured at room temperature for 48 hours. The membrane was further cured at 80 ^{o}C for 2 hours to ensure complete crosslinking and evaporate the remaining hexane.

Fabrication of the UV-active skin selective layers

A $2*10^{-3}$ M solution of **4ASil** was prepared by dissolving a pre-weighed amount of **4ASil** in ethyl acetate. 0.3ml of the solution was then spin coated onto LDPE/PDMS using the dynamic dispense method at 1500 rpm for 45 seconds. The final composite membrane was dried at room temperature under vacuum overnight.

Permeation measurements and de-polymerisation

The gas permeation of the fabricated membranes was tested using an in-house built instrument.

The instrument used a pressure rise method,[2] where the membrane was sealed between a 1 bar feed side and a vacuum permeate side. A pressure transducer measured and recorded the rise in the permeate side pressure. Tests were conducted for pure oxygen feeds at room temperature conditions. Full details on the permeation setup are described in previous literature.[3]

The permeance, P_i, of each membrane was inferred from the change in pressure on the permeate side, with the calculation being:

$$Pi = \frac{Ni}{dPi * A}$$

where N_i (mol s^{-1}) is the is the permeate flow rate of component i, dP_i (Pa) is the transmembrane pressure of component i, and A (m^2) is the membrane area[3].

Characterization

All SEM images were taken on a FEI Nova NanoSEM 450 FEGSEM at an accelerating voltage of 5 kV. A UV-1800 Shimadzu spectrophotometer was used to measure and record UV-Vis results. FT-IR frequencies were measured and recorded using an Agilent Cary 630 FTIR spectrometer, using 32 scans at a resolution of 4 cm^{-1}. Irradiation was performed using a CL1000M UV-cross-linker lamp (UVP LLC., Australia) that provided polychromatic light centred at 365 nm and 254 nm in an open-air environment. H^1 NMR spectra were obtained using a Bruker DRX 400 and 600 instruments. T_g results were obtained using a PerkinElmer DSC-8000 which utilized a nitrogen purge.). The heating rates were: 85 $^oC\ min^{-1}$ for the crosslinked T_g (See main text Fig, 3a), and 40 $^oC\ min^{-1}$ for the de-crosslinked T_g (See main text Fig. 3b). TGA curves were obtained using a Mettler TGA/DSC1 star system. GPC data were obtained using a TOSOH high performance EcoSEC HLC-8320 GPC system. MS results were obtained using an Agilent 6220 TOF MS system, with a multimode dual nebuliser ESI/APCI source. Test compound/s were infused directly into the MS via a kdScientific infusion pump.

Fabrication of porous LDPE

A modified thermally induced phase separation method (TIPS) was used to prepare an asymmetric, macroporous LDPE membrane from raw LDPE films. The method entailed dissolving LDPE in a two-solvent system whose liquids have different volatilities, and LDPE solubilities. When the solution was casted and dried, the polymer-rich phase precipitated as a result of the evaporation of the major, more volatile solvent. Next, the less volatile, minor solvent leaves, which created pores in the membrane.

Experiments were conducted with different solvent ratios of xylene:cyclohexanone, namely 95:5, 90:10, 80:20, and 70:30. It was found that using a cyclohexanone ratio greater than 5 gave rise to a transparent, nonporous film. Therefore, the 95:5 solution ratio was used as the basis for creating the porous LDPE membrane. Fig. S1 shows the high pore density of the membrane, and the magnitude of the pore size.

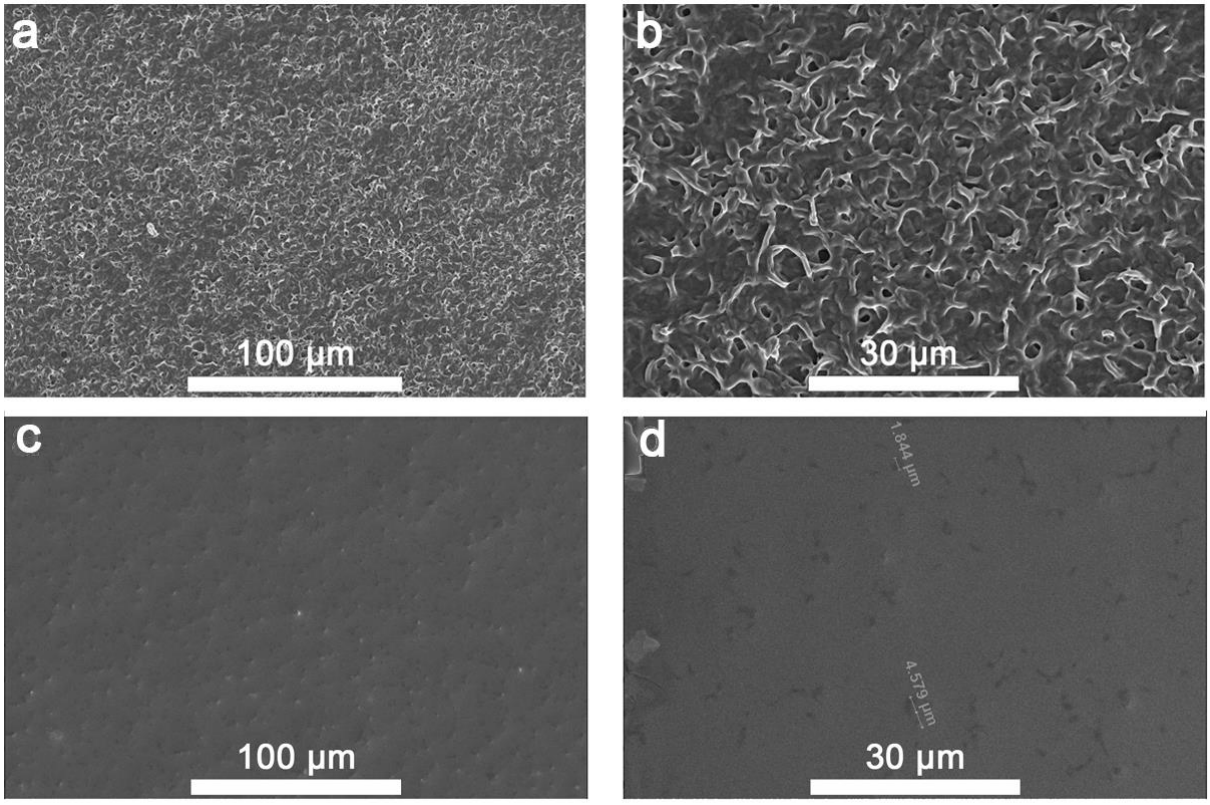

Fig. S1. SEM images of the porous LDPE substrate a) and b), as well as the PDMS gutter layer, c) and d).

4ASil characterisation, physical properties and photoresponsiveness

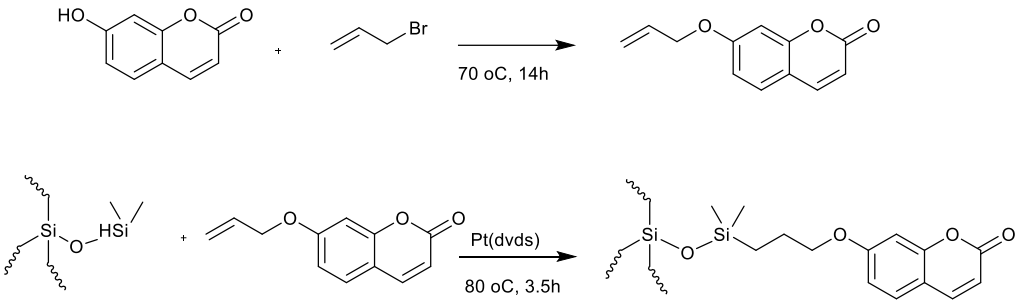

Fig. S2. Synthetic route for **4ASil**. The curled lines represent the remaining 3 arms which have the same chemical structure as the arm shown.

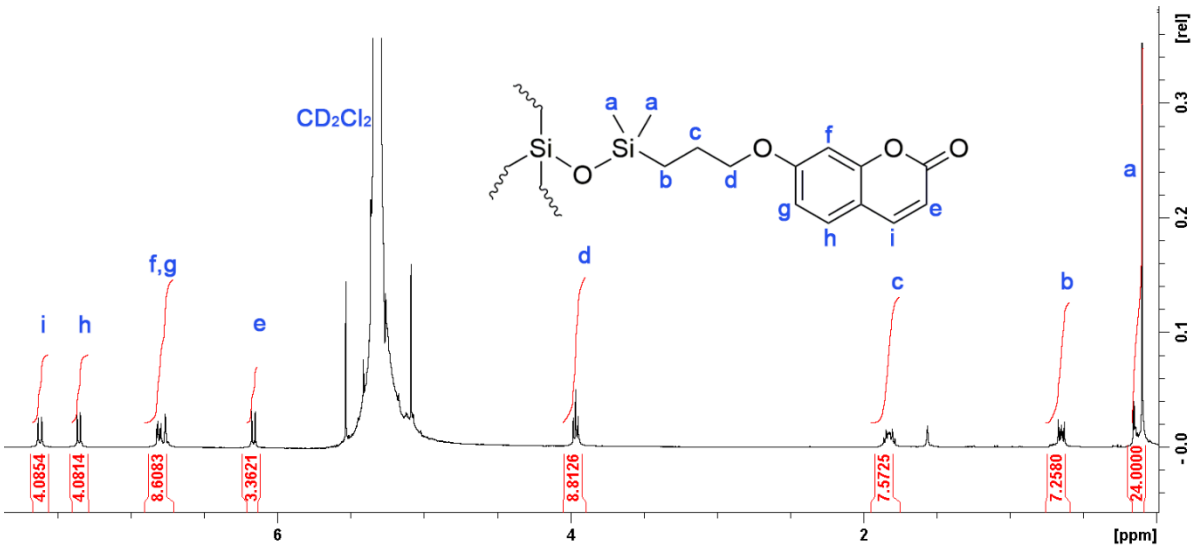

Fig. S3. H^1 NMR spectrum of **4ASil**. Integration is calibrated with respect to the methyl groups' hydrogens on silicon, with 6 per arm, giving a total of 24 hydrogens. Theoretical number of hydrogens for peaks b,c,d, and f,g are 8, while that of e,h, and i are 4. The solvent used was deuterated dichloromethane, or CD_2Cl_2.

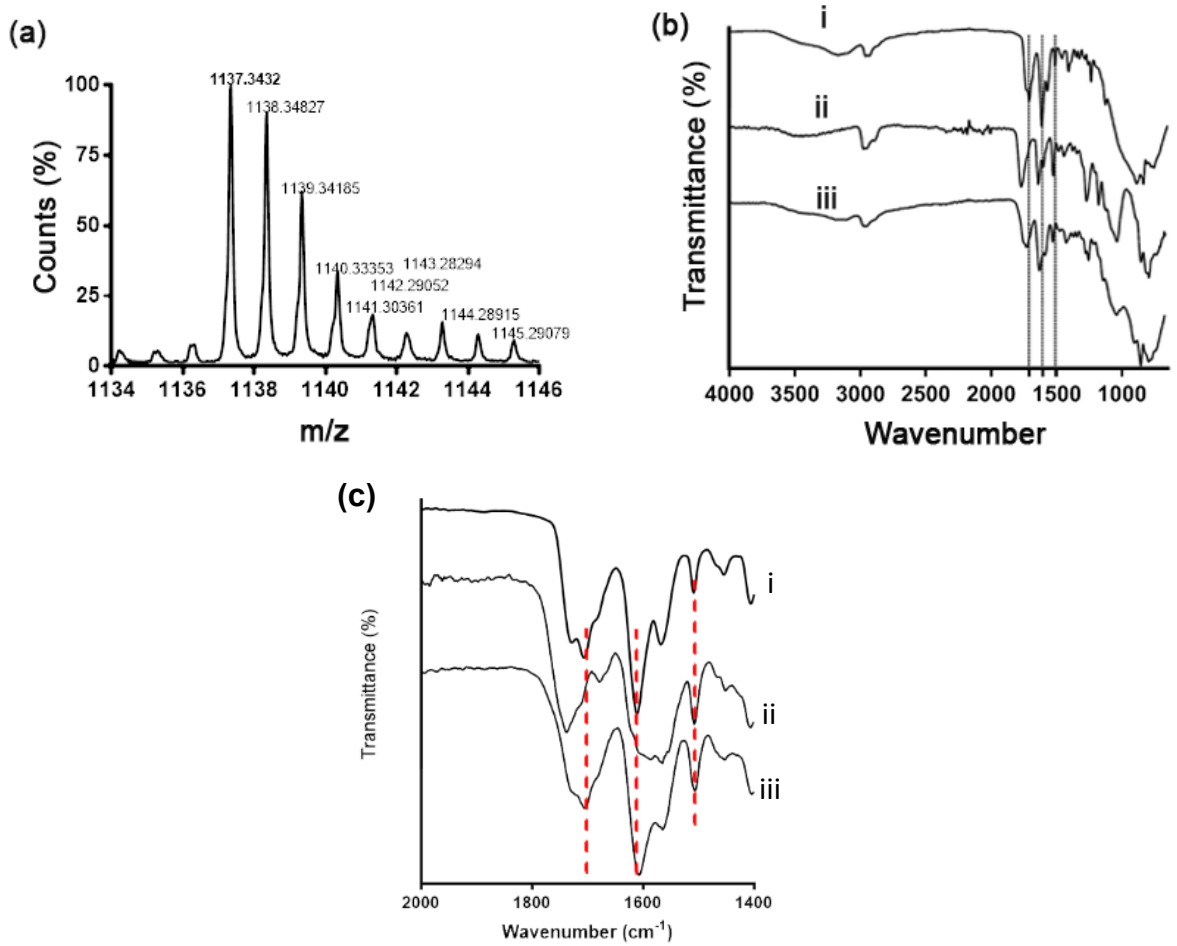

Fig. S4. (a) mass spectrum of **4ASil**. (b) FTIR spectra of **4ASil** as i- monomer, ii- polymer after 365 nm irradiation, iii- de-crosslinked polymer after 254 nm irradiation. (c) Zoomed in plot of (b) at the region of interest, with I,ii, and iii representing the monomer, after crosslinking, and after de-crosslinking

The synthesis of **4ASil** was accomplished by employing a hydrosilylation reaction employing Karstedt's catalyst, as described in Fig. S2. The reaction yield was 99%+ and its structure was confirmed by ^{1}H-NMR. The complete disappearance of the ^{1}H NMR peak at 4.5 corresponding to the Si-H of tetrakis(dimethylsiloxy)silane had indicated that all four arms of the starting silane had reacted. The appearance of peaks around 0.6, 1.8 and 4.0 and their correct integration with respect to Si-CH_3 indicated that all arms had the 7-(propoxy) coumarin attached. Furthermore, the FTIR spectra in Fig. S4b showed no peaks in the region 2080-2280 cm^{-1}, which corresponds to the Si-H group. Finally, the mass spectrum in Fig. S4a gave a reasonable mass spectrum error of 0.52 ppm.

In comparing Fig. S4c(i) monomer and S4c(ii) polymer, observations regarding crosslinking could be made. Firstly, the peak at 1710 cm^{-1} shifted to 1755 cm^{-1}, accompanied by a decrease in intensity, proving a change in the C=O stretching frequency. Secondly, a shift in the 1608 cm^{-1} to 1625 cm^{-1} peak, and the decrease in intensity were seen due to cleavage of the C=C at the 2,3 coumarin carbon sites. Finally, an increase in peak intensity at 1508 cm^{-1} indicated the formation of a cyclic C-C frequency, and hence, the cyclobutane ring. Conversely, irradiation under 254 nm did the exact opposite, as seen in Fig. S4c(iii). The C=O peak at 1710 cm^{-1} reverted back to its original position and intensity, the C=C re-formed by reversion of the 1608 cm^{-1} peak back to a higher intensity and lower shift, and the decrease in peak intensity at 1508 cm^{-1}, which indicated cleavage of the cyclobutane ring.

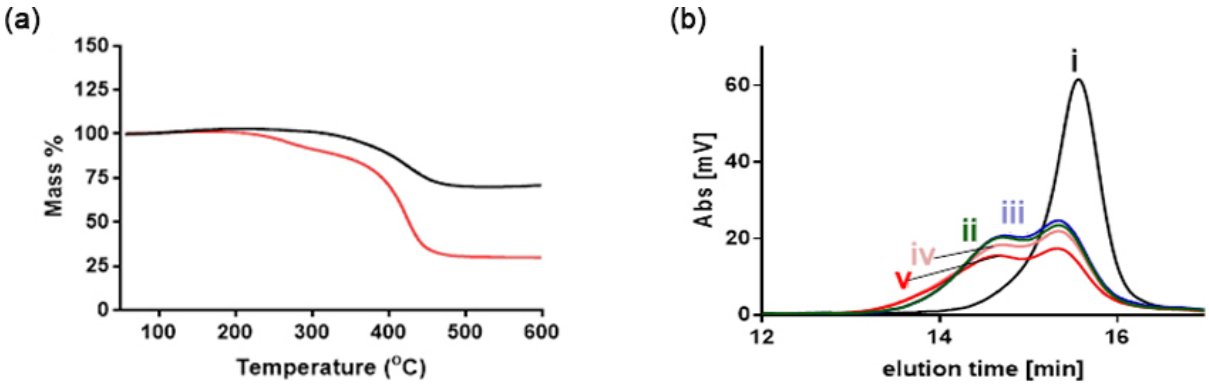

Fig. S5. (a) TGA analysis of the decomposition of **4ASil** as a crosslinked polymer (black), and a monomer (red). The heating rate used was 10 °C min^{-1}. (b) is the raw GPC data of **4ASil**. i- monomer, ii- monomer after 0.04 J cm^{-2} irradiation with 365 nm, iii-v partial polymer after 0.53 - 1.58 J cm^{-2} irradiation with 254 nm at 0.53 J cm^{-2} increments.

While both states of **4ASil** exhibited a similar decomposition temperature of 378 °C, the total mass loss of the monomer was 70%, while that of the crosslinked polymer was 30% (Fig. S5a). Fig. S5b shows the gel permeation chromatography (GPC) spectra of the material after partial crosslinking and de-crosslinking. After polymerization with 365 nm irradiation, a new, lower elution time peak was observed, which was indicative of the formation of a higher molecular weight material. After irradiation with 254 nm, the polydispersity increased, but it was difficult to determine the formation of specific

oligomers as the sample used for the GPC was thicker than the one used for the permeance study, and hence complete de-crosslinking could not happen due to the photomasking effect.

4ACar characterisation and photoresponsiveness

Another star-shaped 4-arm carbon-based monomer **4ACar** was synthesized following a previously described procedure from our group [4] to compare with **4ASil** and show the effect of a tunable T_g on the oxygen permeance.

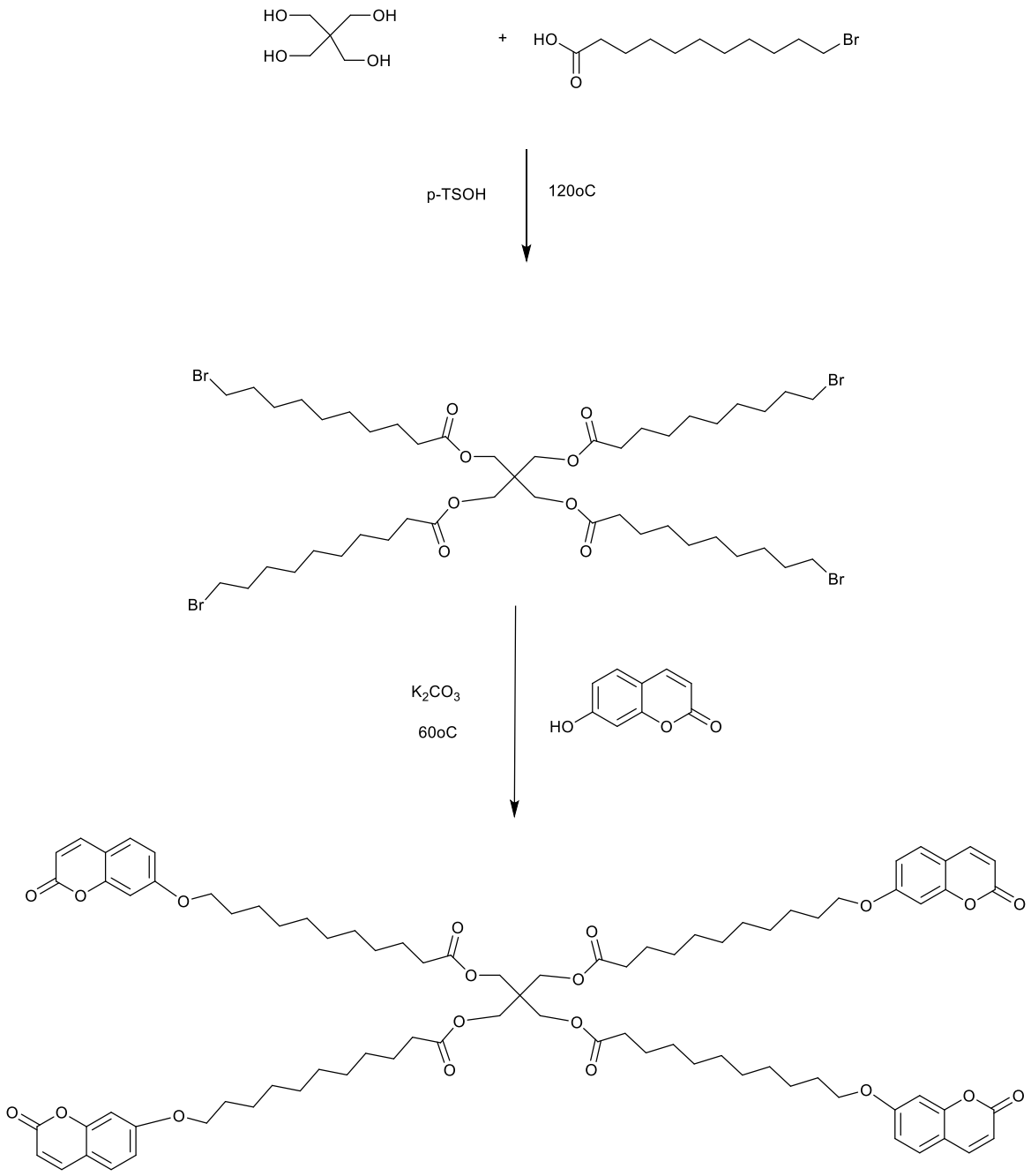

Fig.S6. Synthetic route for **4ACar**.

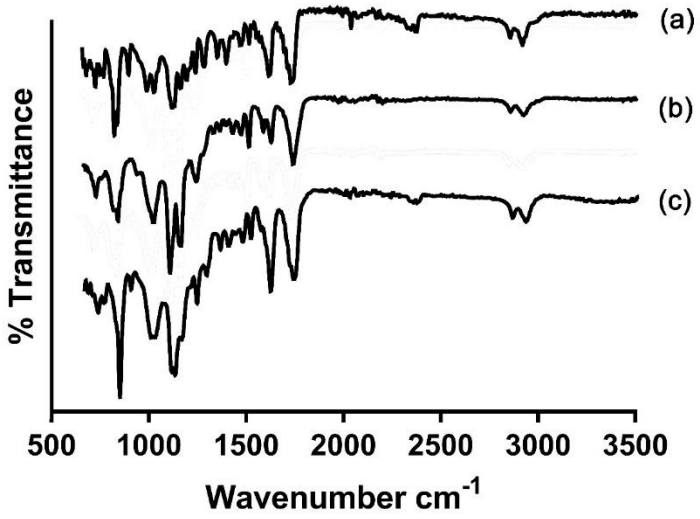

Fig. S7. FTIR results of a 0.1 M spin coating solution of **4ACar** on a glass slide. (a) The monomer absorbance. (b) The crosslinked polymer absorbance after irradiation of (a) with 365 nm UV. (c) The de-crosslinked film absorbance after irradiation of (b) with 254 nm UV. The FTIR peak shifts are identical to that of **4ASil** (see Fig. S4c).

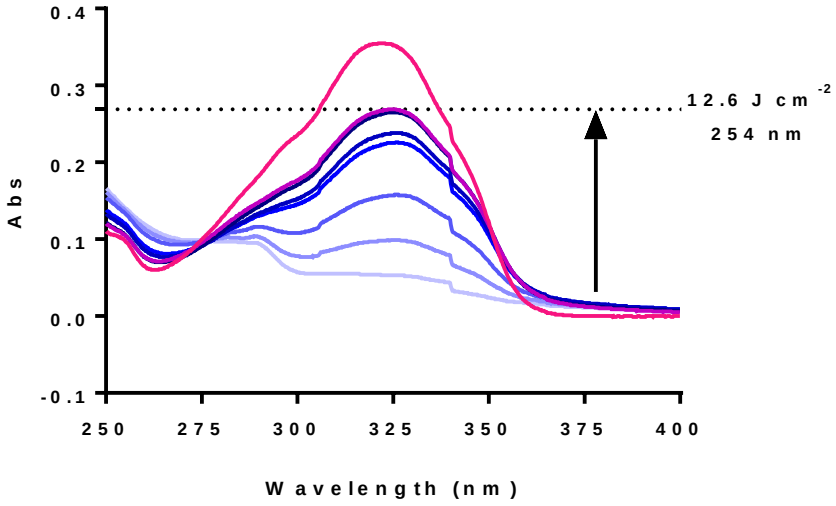

Fig.S8. UV-Vis study of de-polymerisation for a 0.01 M spin coating solution of **4ACar** film. The top line is the monomer, and the bottom is the crosslinked polymer after 11.6 J cm^{-2} irradiation with 365 nm UV light.

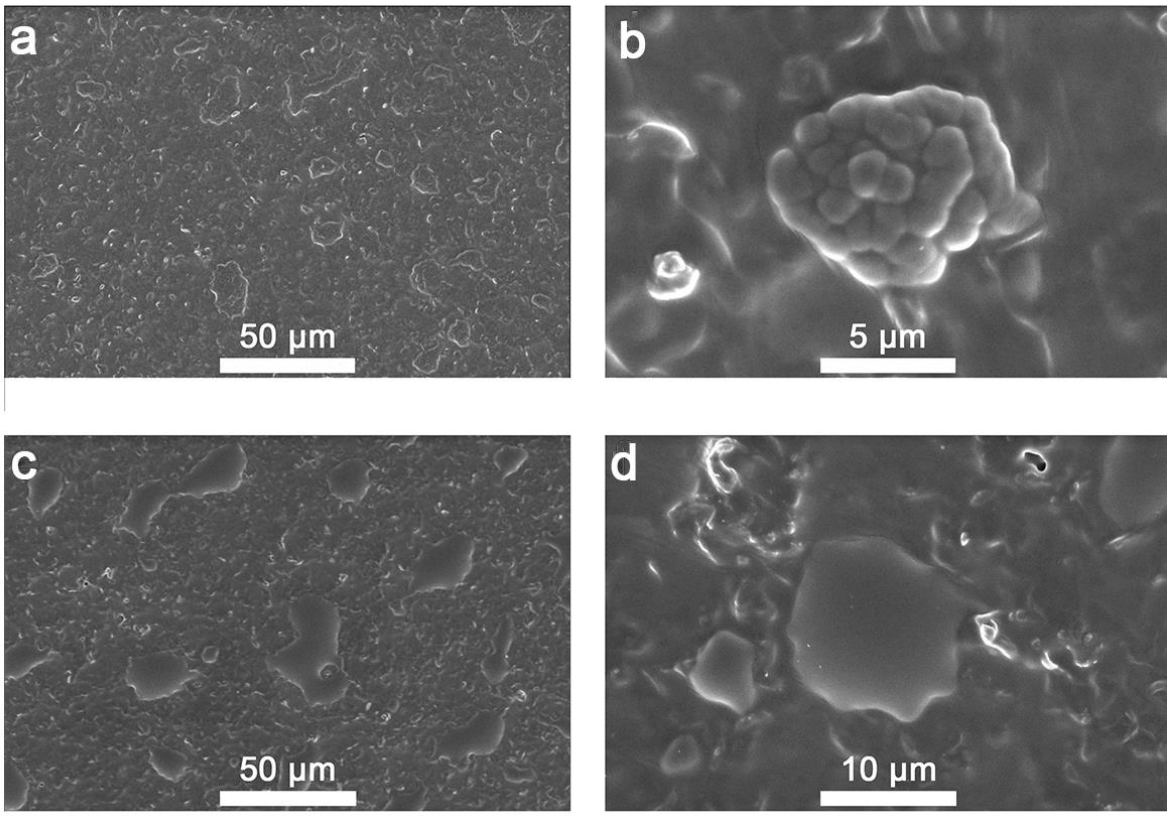

Figure S9. Topological SEM images for different the skin layers after being coated onto PDMS/LDPE: a) and b) are **4ACar** post-polymerisation with 11.60 J cm^{-2} 365 nm light. c) and d) are **4ACar** post-depolymerisation with 9.00 J cm^{-2} 254 nm light. Depolymerisation images were taken after the materials were irradiated with 365 nm (11.6 J cm^{-2}). **4ACar** was fabricated using a 0.02 M spin coating solution.

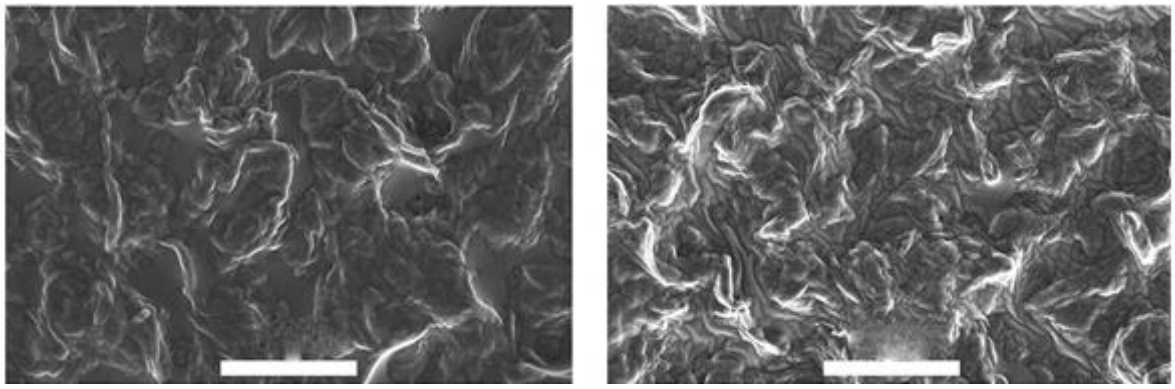

Figure S10. Topological images of **4ASil** after 365 nm irradiation (left) and 254 nm irradiation (right).

Permeability

As part of the study, a star-shaped carbon based monomer, **4ACar**, was synthesized and fabricated to compare the result with **4ASil**. Results proved that the T_g of the de-crosslinked polymer from **4ACar** was too high (37.5 ^oC)[4] to show a permeance change at room temperature conditions. Rather, the film needed a much larger irradiation dose for de-crosslinking than **4ASil**, with experiments concluding that the film needs to be heated above its T_g while de-crosslinking, and then subsequently cooled back to room temperature.

Table S1. Comparison of the changes in oxygen permeance values for **4ACar** and **4ASil** based on irradiation with 365 nm and 254 nm UV light.

Material code	Spin coating solution concentration [M]	UV wavelength [nm]	Irradiation dose [J cm^{-2}]	Permeance [10^{-10} mol m^{-2} s^{-1} Pa^{-1}]
4ACar	0.02	365	11.50	22.9 ± 3.7
		254	12.60	93.5 ± 2.4
	0.025	365	11.50	19.9 ± 3.1
		254	12.60	64.1 ± 2.0
	0.03	365	11.50	16.2 ± 1.5
		254	12.60	49.0 ± 6.1
4ASil	$2x10^{-3}$	365	**0.01**	53.5 ± 0.76
		365	**0.04**	27.8 ± 1.4
		254	**1.05**	70.9 ± 1.3

For **4ACar**, different spin coating solution concentrations were used to analyze the relationship between membrane thickness and permeance. For **4ASil**, it was found that $2x10^{-3}$ M spin coating solution created a film able to undergo permeance reversibility, while using a minimum amount of material without the film tearing under the high vacuum permeance testing conditions. For **4ACar**, 3 samples were tested for each data line. For **4ASil**, 5 samples were tested. As shown **in Fig. S11**, the change in permeance

decreases with increasing spin coating solution concentration, which translates to having a thicker film. This phenomenon was expected due to the photomasking effect, as well as the inversely proportional relationship between permeance and thickness.

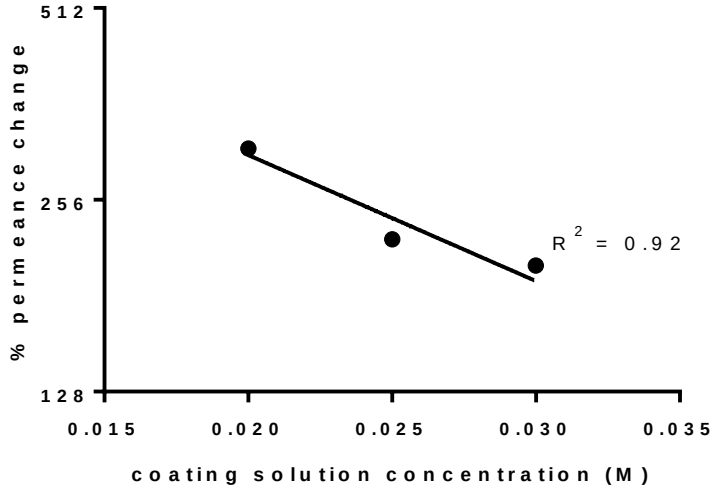

Fig. S11. Graph of the percent change in permeance versus coating solution concentration for 4ACar after 254 nm irradiation with a dose of 12.60 J cm^{-2}.

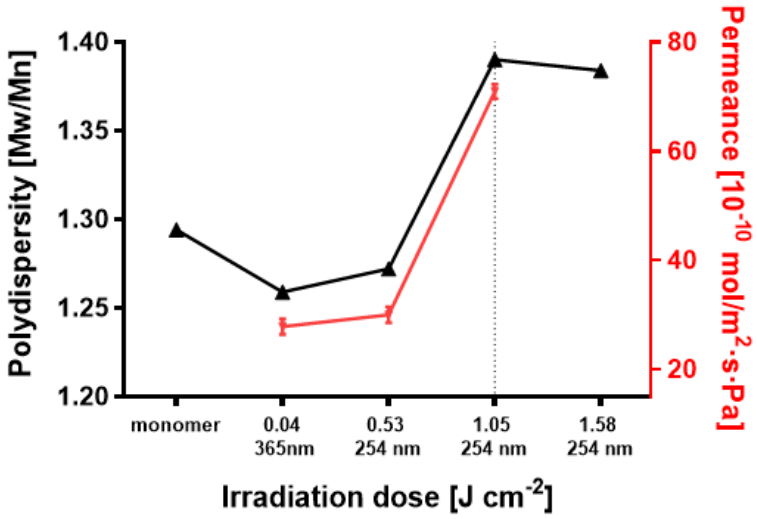

Fig. S12. The relationship between polydispersity of **4ASil** found by GPC and gas permeability, going from a high barrier film with 365 nm to an oxygen permeable membrane with 254 nm irradiation. Polydispersity increase is expected since irradiation with 254 nm causes the formation of oligomers. Hence, a jump in polydispersity seen was indicative of a sharp increase in amount of de-crosslinked polymer. It was observed that the permeance switch occurred at that cutoff.

In Fig. S12, samples of **4ASil** were first partially crosslinked with 0.04 J cm^{-2} by 365 nm irradiation and then de-crosslinked with 254 nm. UV depolymerisation usually causes a reduction in the polymer peak area by GPC (Fig, S5a), but does not cause the material to revert back to its original monomer, but rather forming a mixture of oligomers and monomer. Hence, an increase in polydispersity is to be expected with 254 nm irradiation. It was observed that a sharp increase in polydispersity occurred after 1.05 J cm^{-2} 254 nm, which was also the irradiation dose threshold needed to substantially increase the oxygen permeance of the film. A plausible explanation is that a high barrier property could be retained within a range of amount of crosslinked material in the matrix. Once the amount of crosslinked polymer in the film matrix falls below that range, the film becomes permeable.

Table S2. Pure gas permeance and selectivity for **4ASil**, using a 2x10^{-3} M spin coating solution concentration.

Permeance [10^{-10} mol m^{-2} s^{-1} Pa^{-1}]					Ideal selectivity		
O_2	CO_2	N_2	H_2	CH_4	H_2/N_2	O_2/N_2	H_2/O_2
65	81	97	346	97	3.6	0.7	5.4

Table S2 displays the pure gas permeance values of the composite membrane. 'soft', or rubbery polymers such as **4ASil** show poor molecular sieving abilities, mainly due to the low activation energy required by the penetrant molecules to permeate through the membrane. Hence, it was difficult to find a trend with regards to the gas selectivity of the composite membrane. Naturally, hydrogen showed the highest gas permeance due to having a very small kinetic diameter when compared with the other gases. CO_2 and CH_4 showed a higher value than O_2, as such condensable gases are easily adsorbed by the Si-O bond found in siloxane-based polymers, hence plasticizing them[5].

Crosslinking and T_g relationship with permeability, a theoretical background

To design the photoactive monomer and be able to predict whether a change in crosslinking and T_g via UV induced polymerisation reactions could change the permeability of the nonporous film, a theoretical background was essential.

The most widely accepted mode of transport through nonporous polymer membranes is that of the solution-diffusion model, where gas molecules first adsorb onto the membrane surface, and then diffuse through the membrane, exiting to the downstream side of the membrane.[6,7] The quantification of such phenomena is often a property known as permeability, which is an inherent property of a membrane, and is expressed as:

$$Pi = D_i \times S_i \qquad \text{equation (1)}$$

where P_i is the permeability coefficient of gas i, D_i is the diffusivity, and S_i is the sorption coefficient.[6] In recent years, there has been a shift to quantify a membrane's ability to permeate gas by permeance, which is a factor dependent on membrane thickness, making it a more practical unit of reporting, and can be expressed as:

$$J_i = P_i/L = \frac{N_i}{dP_i \times A} \qquad \text{equation (2)}$$

where L is the membrane thickness, N_i (mol s^{-1}) is the is the permeate flow rate of component i, dP_i (Pa) is the transmembrane pressure of component i, and A (m^2) is the membrane area.[8]

References

1 S. Honda and T. Toyota, *Polymer* 2018, **148**, 211.
2 Z. Zhong, J. Yao, R. Chen, Z. Low, M. He, J. Z. Liu and H. Wang, *J. Mater. Chem. A* 2015, **3**, 15715.
3 L. He, D. Li, D. Dong, J. Yao, Y. Huang and H. Wang, *J. Appl. Polym. Sci.* 2012, **124**, 3383.
4 M. Abdallh, C. Yoshikawa, M.T.W. Hearn, G.P. Simon and K. Saito, Macromolecules 2019, **52**, 2446.
5 T.C. Merkel, *J. Poly. Sci. B* 2000. **38**, 415.
6 T. Li, Y. Pan, K. Peinemann and Z. Lai, J. Memb. Sci. 2013, 425-426, 235.
7 K. Scott, Handbook of Industrial Membranes, Elsevier, New York, NY, USA, 1995.
8 Z. Zhong, J. Yao, R. Chen, Z. Low, M. He, J. Z. Liu and H. Wang, J. Mater. Chem. A 2015, 3, 15715.